A Model for Strongly Nonlinear Long Interfacial Waves with Background Shear

By Anakewit Boonkasame and Paul A. Milewski

The Miyata–Choi–Camassa (MCC) system of equations describing long internal nonhydrostatic and nonlinear waves at the interface between two layers of inviscid fluids of different densities bounded by top and bottom walls is mathematically ill-posed despite the fact that physically stable internal waves are observed matching closely those of MCC. A regularization to the MCC equations that yields a computationally simple well-posed system for time-dependent evolution is proposed here. The regularization is accomplished by keeping the full hyperbolic part of MCC and exchanging spatial and temporal derivatives in one of the linearized dispersive terms. Solitary waves of MCC over a wide range of parameters are used as a benchmark to check the accuracy of the model. Our model includes the possibility of a background shear, and we show that, contrary to the no shear case, solitary waves can cross the midlevel between the top and the bottom walls and may have different polarity from the case with no background shear. Time-dependent solutions of the regularization stable model are presented, including interactions of its solitary waves, and classical and modified Korteweg-de Vries equations for small amplitude waves with the inclusion of background shear are derived. Throughout the paper, the Boussinesq approximation is taken, although the results can be extended to the non-Boussinesq case.

1. Introduction

The atmosphere and the ocean are examples of density-stratified fluids, by which we mean that, at rest densities vary in the vertical. In the ocean, such

Address for correspondence: Paul A. Milewski, Department of Mathematical Sciences, University of Bath, Bath, BA2 7AY, UK; e-mail: p.a.milewski@bath.ac.uk

DOI: 10.1111/sapm.12036

STUDIES IN APPLIED MATHEMATICS 00:1–32

density variation is a result of changes in temperature or salinity. In many cases, there is a height or a depth at which the fluid density changes more abruptly, and internal waves propagate along this density interface. Interfacial waves of this type have been widely observed (see [1, 2]), and often have horizontal length scales much longer than the vertical scale of the flow. Their behavior is an important component of dynamics of the atmosphere and the ocean: propagating internal waves redistribute energy with little dissipation, whereas breaking or unstable internal waves dissipate energy locally and mix the fluid.

The simplest two-dimensional model of internal waves, consisting of two layers of inviscid fluids bounded by top and bottom walls has been studied extensively in previous works. In cases where the typical length scales of internal waves are much larger than the depths of both fluid layers, it is customary to make the long-wave (or shallow water) assumption to simplify the governing Euler equations [3–5]. In these earlier works, either hydrostatic or small-amplitude assumptions were made. To describe the observed internal waves of large amplitude, it is important to include fully nonlinear and nonhydrostatic effects [6–8]. A well-known fully nonlinear long-wave model, which contains dispersive terms arising from nonhydrostatic pressure corrections, is the Miyata–Choi–Camassa (MCC) system [7, 9]. While solitary-wave solutions of this system show good agreement with observations [10–12], it is of limited use as a time-dependent model, because it is mathematically ill-posed [13], despite the fact that physically stable internal waves of large amplitude have been observed [14].

We shall study a fully nonlinear long-wave system obtained from the MCC system by making the Boussinesq approximation; that is, we assume that the difference in the fluid densities is small compared to the mean density such that the density difference affects buoyancy but not inertia. Like the MCC system, this Boussinesq MCC system is nonhydrostatic and dispersive, and it is ill-posed under small perturbations of sufficiently high wavenumbers. Ill-posedness in shallow-water interfacial wave equations can arise *either* out of the mathematical manifestation of the long-wave limit of the Kelvin–Helmholtz (KH) instability [15], *or* as an "unphysical" consequence of the truncation of the problems' dispersion relation in the long-wave regime. (The latter issue also occurs in surface wave modeling [16].)

In the systems that we consider, *both* of these occur and one must therefore remove the unphysical instability due to the truncation while preserving the physical KH instability properties of long waves if the shear is sufficiently strong. This is achieved by an asymptotically consistent regularization exchanging spatial and temporal derivatives in a dispersive term, to obtain a region in the phase plane in which the system is stable. Two regularizations are proposed: a linear and a nonlinear one. The linear regularization results in a cubically nonlinear Boussinesq system that is numerically far simpler to solve than MCC. Both regularizations can be used to describe general flows with nonzero

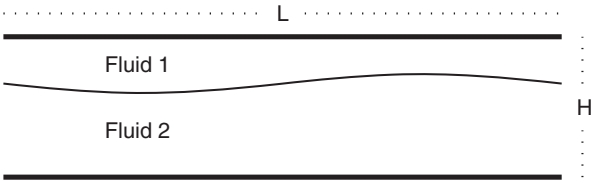

Figure 1. Two layers of fluids bounded by top and bottom walls. The subscripts $j = 1$ and $j = 2$ below indicate the upper and lower fluids, respectively.

mean (or far-field) shear. (See [17] for another approach at deriving quadratic and cubic Boussinesq equations modeling interfacial waves.)

The steady solitary waves of the new stable model are compared to those of the Boussinesq MCC, since, in the case of zero far-field shear, MCC solutions compare well with experiments [12]. The comparisons show that the agreement is generally excellent, and several new qualitative features of large amplitude internal waves *with* background shear are captured. It is known that under the Boussinesq approximation and without background shear, internal solitary waves for the MCC system cannot cross the midlevel between the top and the bottom walls and that solitary waves of depression type are possible only when the lower fluid layer is thicker than the upper fluid layer. These types of results are extended to the case with background shear, and we conclude that the level which solitary waves cannot cross depends on both their direction of propagation and the strength of the shear. As a result, stable solitary waves of elevation type are also possible when the lower fluid layer is thicker than the upper fluid layer in the presence of sufficiently strong (yet stable in the sense of long-wave KH) background shear. Background shear was included in a study of *periodic* internal waves of MCC in [18].

This paper is organized as follows. In Section 2, we present a formulation of the fully nonlinear long-wave MCC system with the Boussinesq approximation. Then, in Section 3, it is shown that this system is not linearly stable. In Section 4, a new stable model is obtained by an exchange of spatial and temporal derivatives in a dispersive term of the unstable system. We compare solitary waves of the unstable system and the stable model in Section 5 as well as consider time-dependent solutions of the stable model. In Sections 6, using small amplitude approximations, we obtain classical and modified Korteweg-de Vries (KdV) equations for the models.

2. Formulation

Consider incompressible, irrotational two-dimensional flows in two layers of ideal fluids bounded by horizontal top and bottom walls as shown in Figure 1.

Assuming that the separation H between the walls is much smaller than the typical horizontal length scale L of internal waves, define $\mu \equiv H/L \ll 1$ as the shallow-water parameter.

The nondimensional physical quantities together with their scalings shown in brackets are

- H_j $[\times H]$ heights of undisturbed fluid layers,
- ρ_j $[\times \bar{\rho}]$ fluid densities,
- τ $[\times L/\sqrt{gH}]$ for time,
- x $[\times L]$ horizontal position,
- y $[\times H]$ vertical position, measured from undisturbed interface,
- $h_j(\tau, x)$ $[\times H]$ heights of fluid layers,
- $u_j(\tau, x, y)$ $[\times \sqrt{gH}]$ horizontal fluid velocity,
- $v_j(\tau, x, y)$ $[\times \mu\sqrt{gH}]$ vertical fluid velocities,
- $P_j(\tau, x, y)$ $[\times \bar{\rho} gH]$ pressures within the fluids.

Here, $\bar{\rho}$ is the mean density and g is the acceleration due to gravity. As a result of the scalings,

$$\frac{\rho_1 + \rho_2}{2} = 1 \qquad \text{and} \qquad h_1 + h_2 = 1.$$

The Euler equations governing the flow are

$$u_{j,x} + v_{j,y} = 0, \tag{1}$$

$$\mu^2 v_{j,x} - u_{j,y} = 0, \tag{2}$$

$$\rho_j(u_{j,\tau} + u_j u_{j,x} + v_j u_{j,y}) = -P_{j,x}, \tag{3}$$

$$\mu^2 \rho_j(v_{j,\tau} + u_j v_{j,x} + v_j v_{j,y}) = -P_{j,y} - \rho_j. \tag{4}$$

The boundary conditions are that vertical components of fluid velocities vanish on the top and bottom walls,

$$v_1 = 0 \quad \text{at} \quad y = H_1 \qquad \text{and} \qquad v_2 = 0 \quad \text{at} \quad y = -H_2, \tag{5}$$

the kinematic conditions at the interface

$$h_{1,\tau} + h_{1,x}u_1 = -v_1 \quad \text{and} \quad h_{2,\tau} + h_{2,x}u_2 = v_2, \quad \text{at } y = H_1 - h_1 = h_2 - H_2, \tag{6}$$

and the dynamic condition of continuity of pressures at the interface

$$P_1 = P_2 \equiv P(\tau, x) \qquad \text{at} \qquad y = H_1 - h_1 = h_2 - H_2. \tag{7}$$

Since (2) implies small vertical variations in u_j, it is usual to consider their vertical averages

$$\bar{u}_1(\tau, x) \equiv \frac{1}{h_1} \int_{H_1 - h_1}^{H_1} u_1 \, dy \qquad \text{and} \qquad \bar{u}_2(\tau, x) \equiv \frac{1}{h_2} \int_{-H_2}^{h_2 - H_2} u_2 \, dy,$$

and study the time evolution of h_j, $\bar{u}_j$, and P, which are functions of τ and x only.

Vertically integrating (1) and using the boundary conditions (5) and (6) yield conservation of mass (or volume) in each fluid layer

$$h_{1,\tau} + (h_1 \bar{u}_1)_x = 0, \tag{8}$$

$$h_{2,\tau} + (h_2 \bar{u}_2)_x = 0. \tag{9}$$

It follows from (2) that $u_j = \bar{u}_j + O(\mu^2)$ and hence that $\overline{u_j^2} = \bar{u}_j^2 + O(\mu^4)$. (This can be *assumed* without an explicit assumption of exact irrotationality.) Vertically integrating (4) using this estimate and (7) yield expressions for the pressures to $O(\mu^2)$

$$P_1 = P + \rho_1 (H_1 - h_1 - y) - \frac{\mu^2 \rho_1}{2} \left[h_1^2 - (H_1 - y)^2 \right] F_1, \tag{10}$$

$$P_2 = P + \rho_1 (h_2 - H_2 - y) - \frac{\mu^2 \rho_2}{2} \left[(H_2 + y)^2 - h_2^2 \right] F_2, \tag{11}$$

where $F_j \equiv \bar{u}_{j,x\tau} + \bar{u}_j \bar{u}_{j,xx} - (\bar{u}_{j,x})^2$. The $O(\mu^2)$ terms in (10) and (11) are nonhydrostatic corrections of the hydrostatic pressure. Substituting these expressions for P_j into (3) and vertically averaging, it gives

$$\rho_1 \left[\bar{u}_{1,\tau} + \bar{u}_1 \bar{u}_{1,x} - h_{1,x} - \frac{\mu^2}{3h_1} \left(h_1^3 F_1 \right)_x \right] = -P_x, \tag{12}$$

$$\rho_2 \left[\bar{u}_{2,\tau} + \bar{u}_2 \bar{u}_{2,x} + h_{2,x} - \frac{\mu^2}{3h_2} \left(h_2^3 F_2 \right)_x \right] = -P_x. \tag{13}$$

The system consisting of (8)–(9), (12)–(13), and the constraint $h_1 + h_2 = 1$ governs the evolution of the fluids and is called the MCC system.

Adding (8) and (9) yields $(h_1 \bar{u}_1 + h_2 \bar{u}_2)_x = 0$, which defines the *volume flux*

$$Q(\tau) \equiv h_1 \bar{u}_1 + h_2 \bar{u}_2,$$

which is independent of x. In general,

$$Q' = \left[\frac{h_1^2}{2} - \frac{h_2^2}{2} - h_1 \bar{u}_1^2 - h_2 \bar{u}_2^2 + \frac{\mu^2}{3} \left(h_1^3 F_1 + h_2^3 F_2 \right) \right]_x - \left(\frac{h_1}{\rho_1} + \frac{h_2}{\rho_2} \right) P_x,$$

and unless the Boussinesq approximation is made (i.e., setting $\rho_1 = \rho_2$ in the last term, resulting in a local expression for the pressure) $Q' \neq 0$ in general. For details and a complete discussion, see [15].

We now make the Boussinesq approximation, by replacing ρ_1 and ρ_2 in inertia terms by the mean (unit) density in (12)–(13), and consider only cases in which far-field conditions fix $Q = 0$ (a constant Q can then be removed by a Gallilean transformation). Thus, (12) and (13) become

$$\bar{u}_{1,\tau} + \bar{u}_1 \bar{u}_{1,x} - \rho_1 h_{1,x} - \frac{\mu^2}{3h_1}\left(h_1^3 F_1\right)_x = -P_x, \tag{14}$$

$$\bar{u}_{2,\tau} + \bar{u}_2 \bar{u}_{2,x} + \rho_2 h_{2,x} - \frac{\mu^2}{3h_2}\left(h_2^3 F_2\right)_x = -P_x. \tag{15}$$

To reduce (8)–(9) and (14)–(15) to a system of two equations, subtract (8) from (9) and (14) from (15) and write the resulting equations in terms of new displacement–shear variables

$$h \equiv h_2 - h_1, \qquad w \equiv \frac{\bar{u}_2 - \bar{u}_1}{\sqrt{\rho_2 - \rho_1}}, \qquad t \equiv \frac{\tau\sqrt{\rho_2 - \rho_1}}{2},$$

which yields the nonhydrostatic system of equations

$$h_t + \left[(1 - h^2)w\right]_x = 0, \tag{16}$$

$$w_t + \left[(1 - w^2)h\right]_x = \frac{\mu^2}{24}\left(\frac{1}{1+h}\left[(1+h)^3 G_2\right]_x - \frac{1}{1-h}\left[(1-h)^3 G_1\right]_x\right), \tag{17}$$

where

$$G_1 \equiv -\left[(1+h)w\right]_{xt} + \left[(1+h)w\right]\left[(1+h)w\right]_{xx} - \left(\left[(1+h)w\right]_x\right)^2,$$

$$G_2 \equiv \left[(1-h)w\right]_{xt} + \left[(1-h)w\right]\left[(1-h)w\right]_{xx} - \left(\left[(1-h)w\right]_x\right)^2.$$

This system, which we denote as the Boussinesq MCC system, will be considered henceforth.

3. Linear stability and the stable model

In order to study the stability of the Boussinesq MCC system in the presence of small disturbances, (16) and (17) are linearized around constant states h_0

and w_0, to obtain

$$h_t - 2h_0 w_0 h_x + \left(1 - h_0^2\right) w_x = 0, \tag{18}$$

$$w_t + \left(1 - w_0^2\right) h_x - 2h_0 w_0 w_x = -\frac{\mu^2}{12}\left[2h_0 w_0 h_{xxt} - \left(1 - h_0^2\right) w_{xxt} + \left(1 - h_0^2\right) w_0^2 h_{xxx}\right]. \tag{19}$$

Seeking nontrivial solutions of (18) and (19) proportional to $e^{i(kx-\omega t)}$ yields a dispersion relation

$$\omega^2 + 4h_0 w_0 k\omega - \alpha k^2 + \frac{\mu^2}{12}\left(1 - h_0^2\right) k^2 \left[\omega^2 + \left(1 - h_0^2\right) w_0^2 k^2\right] = 0, \tag{20}$$

where

$$\alpha(h_0, w_0) \equiv \left(1 - h_0^2\right)\left(1 - w_0^2\right) - 4h_0^2 w_0^2.$$

Requiring that ω be real, we have the condition

$$1 - w_0^2 + \frac{(\mu k)^2}{12}\left[\alpha - \left(1 - h_0^2\right) w_0^2\right] - \frac{(\mu k)^4}{144}\left(1 - h_0^2\right)^2 w_0^2 \geq 0, \tag{21}$$

which fails for sufficiently high μk when the background shear w_0 is nonzero (note that $1 - h_0^2 > 0$). Thus, the nonhydrostatic system is linearly unstable at high wavenumbers and mathematically ill-posed. This has been noted before and some possible resolutions to the problem have been proposed [13, 19]. Note that even when $w = 0$ initially, it is clear that in (16) and (17), w will not remain zero and thus high-frequency oscillations will become unstable due to the linearized behavior about the new nonzero state. Nevertheless, the hydrostatic problem $\mu^2 = 0$ is *nonlinearly well-posed* for $|w| < 1$ [20]. This change in character between the two models (weakly nonhydrostatic long waves and hydrostatic waves) does not arise out of the physics of the problem since the *full* linear nonhydrostatic problem, when μk is small, is stable depending on a Richardson criterion. Spurious instabilities arise out of a particular truncation in μ^2 of the problem that does not reflect the physics of the KH instability.

3.1. Linear stability of two-layer flows

In order to see this relationship, consider the linear nonhydrostatic problem (i.e., the stability of a vortex sheet between fluids of different densities bounded above and below by walls). The problem is posed as potential flow in the two regions $H_1 > y > 0$ and $0 > y > -H_2$ subject to no flow through $y = H_1$ and $y = -H_2$ and the interfacial conditions linearized about $y = 0$:

$$\eta_t + U_1 \eta_x = \phi_{1,y},$$

$$\eta_t + U_2\eta_x = \phi_{2,y},$$

$$\rho_1\left[\phi_{1,t} + U_1\phi_{1,x}\right] - \rho_2\left[\phi_{2,t} + U_1\phi_{2,x}\right] = g(\rho_2 - \rho_1)\eta,$$

where η is the free surface displacements and U_1, U_2 are the constant horizontal flows in each layer and ϕ_1, ϕ_2 are the perturbation velocity potentials from these uniform flows. The equations are solved by assuming

$$\phi_1 = \frac{1}{ik}\cosh[k(y - H_1)]Ae^{i(kx-\omega t)},$$

$$\phi_2 = \frac{1}{ik}\cosh[k(y + H_2)]Be^{i(kx-\omega t)},$$

$$\eta = Ce^{i(kx-\omega t)},$$

which satisfies Laplace's equations in both regions with the no flow conditions at the rigid boundaries. Substitution into the interfacial conditions yields

$$(U_1 - c)kC - \sinh(kH_1)A = 0, \tag{22}$$

$$(U_2 - c)kC + \sinh(kH_2)B = 0, \tag{23}$$

$$\rho_1(U_1 - c)\cosh(kH_1)A - \rho_2(U_2 - c)\cosh(kH_2)B - g(\rho_2 - \rho_1)C = 0. \tag{24}$$

The condition for a nontrivial solution results in the dispersion relation for the system

$$(U_1 - c)^2kC_1S_2 + (U_2 - c)^2kC_2S_1 - \tilde{g}S_1S_2 = 0, \tag{25}$$

where $S_j = \sinh(kH_j)$, $C_j = \cosh(kH_j)$, the Boussinesq approximation has been made in (24) by setting $\rho_1 = \rho_2 = \rho$ in the terms not involving g, and $\tilde{g} = g(\rho_2 - \rho_1)/\rho$, where ρ is the reference density. We now can set $\tilde{g} = 1$ by rescaling of c and U_j.

It is evident that (i) there are no real solutions for c for fixed k, H_j if $|U_2 - U_1|$ is sufficiently large, (ii) there are no real solutions fixing U_j, H_j with $U_2 - U_1 \neq 0$, in the limit $k \to \infty$. These statements are the mathematical manifestation of the KH shear instability. However, when we study the small k limit, we find: (i) in the $k = 0$ limit, real solutions exist provided $|U_2 - U_1| < 1$; (ii) for k small, the condition for real solutions of the problem depends *crucially* on the details of the truncation.

The quadratic equation for c is

$$\alpha c^2 + \beta c + \gamma = 0,$$

where

$$\alpha = k(C_1 S_2 + C_2 S_1),$$

$$\beta = -2k(U_1 C_1 S_2 + U_2 C_2 S_1),$$

$$\gamma = k\left(U_1^2 C_1 S_2 + U_2^2 C_2 S_1\right) - S_1 S_2.$$

The discriminant, whose sign determines the stability threshhold, is given by

$$4k^2 S_1 S_2 \left[\frac{1}{k}(C_1 S_2 + C_2 S_1) - (U_2 - U_1)^2 C_1 C_2\right]$$

In the long-wave approximation, this system can be expanded in small k and truncated and the sign of the discriminant depends on the sign of:

$$\begin{aligned} 1 \ & -W^2 + \frac{1}{6}k^2\left(1 - 3W^2\left(H_1^2 + H_2^2\right)\right) \\ & + \frac{1}{120}k^4\left(1 - 5W^2\left(H_1^4 + 6H_1^2 H_2^2 + H_2^4\right)\right) + \cdots \end{aligned}$$

The quantities can be expressed in the variables used in the paper with:

$$\begin{aligned} H_1 &= \frac{1}{2}(1 - h_0), \quad H_2 = \frac{1}{2}(1 + h_0), \\ U_1 &= -\frac{1}{2}(1 + h_0)w_0, \quad U_2 = \frac{1}{2}(1 - h_0)w_0, \end{aligned}$$

resulting in

$$1 - w_0^2 + \frac{1}{6}k^2\left(1 - \frac{3}{2}w_0^2\left(1 + h_0^2\right)\right) + \frac{1}{120}k^4\left(1 - \frac{5}{2}w_0^2\left(1 + h_0^4\right)\right) + \cdots$$

At each order, one obtains a Richardson criterion:

$$1 - w_0^2 > 0, \quad 1 - \frac{3}{2}w_0^2\left(1 + h_0^2\right) > 0, \ldots, 1 - \frac{(2n+1)}{2}w_0^2\left(1 + h_0^{2n}\right) > 0, \cdots.$$

Note that those criteria yield "nesting" regions in the (h_0, w_0) plane and therefore if the nth cirterion is satisfied, thus are all the previous ones.

Suppose now that we truncate Equations (22)–(24) each to the first two terms in Taylor series in k. The stability depends on the sign of a discriminant that can be found to depend on the sign of

$$1 - w_0^2 + \frac{1}{4}k^2(1+h_0^2)\left(\frac{4}{3} - w_0^2\right) + \frac{1}{64}k^4(1-h_0^2)^2\left(\frac{2}{3} - w_0^2\right).$$

The interpretation is that the truncated *equations* have a larger stability region than the full dispersion relation truncated to the same order. Furthermore, note that the assumed form of ϕ_j implies that A, B are proportional to the velocities at the walls $y = H_1, -H_2$. In this case, the calculation above shows that a quadratic truncation of the equations is *stable* for $w_0^2 < 2/3$. This calculation confirms the result of [19] whereby, using wall variables, the MCC equations were stabilized.

Suppose the calculation is repeated with variables that reflect the mean velocity in each layer, that is, the traditional MCC variables. Then,

$$\phi_1 = -i\frac{H_1}{\sinh(kH_1)}\cosh[k(y-H_1)]Ae^{i(kx-\omega t)},$$

$$\phi_2 = -i\frac{H_2}{\sinh(kH_2)}\cosh[k(y+H_2)]Be^{i(kx-\omega t)},$$

$$\eta = Ce^{i(kx-\omega t)}.$$

Now, substituting in the dynamic and kinematic conditions, we obtain

$$(U_1 - c)C - H_1 A = 0,$$

$$(U_2 - c)C + H_2 B = 0,$$

$$(U_1 - c)\coth(kH_1)A - (U_2 - c)\coth(kH_2)B - C = 0.$$

Note that the first two equations above are *independent* of k. This is a consequence of using the mean velocity and renders mass conservation (or the kinematic condition) exact to all orders. The condition for nontrivial solutions has the form:

$$(U_1 - c)^2 kH_1H_2\coth(kH_1) + (U_2 - c)^2 kH_1H_2\coth(kH_2) - \tilde{g}H_1H_2 = 0.$$

The solutions are of course *identical* to those of (25); however, this will not be the case upon truncation. The discriminant of the quadratic for c, with $Q_1 = (kH_1)\coth(kH_1)$ and $Q_2 = (kH_2)\coth(kH_2)$, is

$$4H_1H_2\left[(H_2Q_1 + H_1Q_2) - (U_2 - U_1)^2 Q_1Q_2\right].$$

Expanding *each* term Q_j in the brackets to order k^2, which is equivalent to expanding only the dynamic boundary condition, we have that stability depends on the sign of

$$1 - w_0^2 + \frac{1}{12}k^2\left(\left(1 - h_0^2\right) - 2\left(1 + h_0^2\right)w_0^2\right) - k^4\frac{1}{144}\left(1 - h_0^2\right)^2 w_0^2.$$

This is equivalent to the condition found in the previous section and is unconditionally unstable for $w_0 \neq 0$.

The foregoing calculations could be repeated using the velocity at arbitrary levels y_1, y_2 with:

$$\phi_1 = \frac{1}{ik}\cosh^{-1}[k(y_1 - H_1)]\cosh[k(y - H_1)]Ae^{i(kx-\omega t)},$$

$$\phi_2 = \frac{1}{ik}\cosh^{-1}[k(y_2 - H_2)]\cosh[k(y + H_2)]Be^{i(kx-\omega t)},$$

$$\eta = Ce^{i(kx-\omega t)}.$$

While this may lead to interesting conditions, it is beyond the scope of the paper.

3.2. The stable model

There are a number of possible remedies to regularize the MCC equations. One may use a numerical filter for high wavenumbers, thus damping the unstable frequencies, or regularize the equations consistently with the underlying physics. In [19], for example, a stable model is formulated in terms of values of u_1 and u_2 at the top and bottom walls, respectively, as opposed to their vertical averages $\bar{u}_1$ and $\bar{u}_2$ used here. Here, an alternative is proposed, based on exchanges between time and space derivatives used to regularize surface wave equations (see [16]).

It is clear that the condition (21) fails because the coefficient of k^4 is negative. In the process of obtaining the dispersion relation (20), we see that k^4 arises from the terms w_x in (18) and h_{xxx} in (19). Since the latter is much smaller than the former, we can obtain a stable model by modifying this term as follows. By ignoring the right-hand side of (19), we can solve this equation and (18) for h_x in terms of h_t and w_t with an $O(\mu^2)$ error as

$$h_x = \frac{1}{\alpha}\left[2h_0 w_0 h_t + (1 - h_0^2)w_t\right], \tag{26}$$

thus obtaining an exchange of spatial and temporal derivatives. Using (26) to find h_{xxx}, we can rewrite (19) with an $O(\mu^4)$ error as

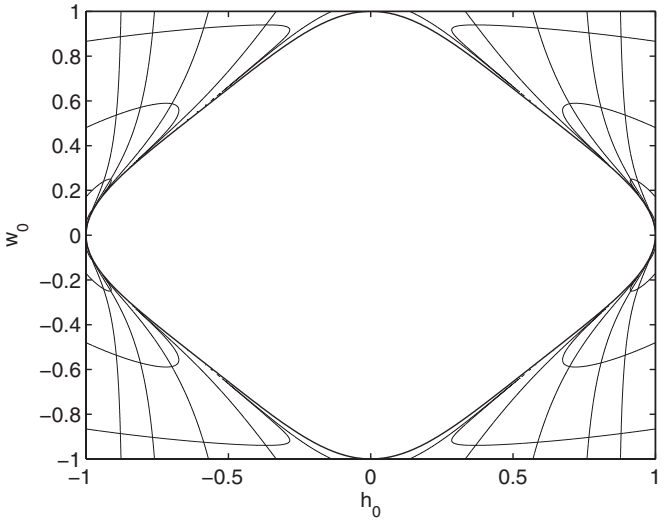

Figure 2. The stable region (the central part of the diagram) for the system consisting of (28) and (29). The nondispersive equations obtained with $\mu^2 = 0$ are stable in the full square $|w_0| < 1, |h_0| < 1$.

$$w_t + \left(1 - w_0^2\right) h_x - 2h_0 w_0 w_x = \\ -\frac{\mu^2}{12}\left[2h_0 w_0 (1-\beta) h_{xxt} - \left(1 - h_0^2\right)(1+\beta) w_{xxt}\right], \tag{27}$$

where

$$\beta(h_0, w_0) \equiv \frac{\left(1 - h_0^2\right) w_0^2}{\alpha}.$$

The system consisting of (18) and (27) has the dispersion relation

$$\omega^2 + 4h_0 w_0 k\omega - \alpha k^2 + \frac{\mu^2}{12}\left(1 - h_0^2\right) k^2 \omega\left[(1+\beta)\omega + 4h_0 w_0 \beta k\right] = 0.$$

Requiring that ω be real, we have the condition

$$\Delta_{\mu k}(h_0, w_0) \equiv 1 - w_0^2 + \frac{(\mu k)^2}{12}\left[\alpha(1+\beta) + 8h_0^2 w_0^2 \beta\right] \\ + \frac{(\mu k)^4}{36}\left(1 - h_0^2\right) h_0^2 w_0^2 \beta^2 \geq 0.$$

It is straightforward to determine that the region on the (h_0, w_0) plane in which this condition holds for all μk satisfies the inequality $\alpha \geq 0$. Its boundary, given by $\alpha = 0$, is precisely the envelope of the family of curves $\Delta_{\mu k} = 0$ as shown in Figure 2.

Our main stable model is a modification of the Boussinesq MCC (16)–(17) by replacing its dispersive terms with those from the right-hand side of (27). This yields

$$h_t + \left[(1-h^2)w\right]_x = 0, \tag{28}$$

$$w_t + \left[(1-w^2)h\right]_x = -\frac{\mu^2}{12}\left[2h_0 w_0(1-\beta)h_{xxt} - (1-h_0^2)(1+\beta)w_{xxt}\right]. \tag{29}$$

In the Appendix, we obtain a second stable model with *nonlinear* dispersive terms—unlike linear ones in (29)—by performing a more general exchange of spatial and temporal derivatives. While this alternative model is more formally consistent, its complexity makes it less practical for computation. We will find that the omission of higher order dispersive terms in (29) does not introduce large errors in the Boussinesq MCC.

For simplicity, we set $\mu^2 = 1$ in the remainder of the paper. While this can be accomplished formally by appropriate rescalings of t and x, the validity of the equations in describing the physical problem is only preserved if the dispersive terms are small.

4. Solitary waves

We wish to see how closely the stable model (28)–(29) approximates the Boussinesq MCC (16)–(17). Obviously, comparing their time-dependent solutions is out of the question, because the Boussinesq MCC is ill-posed. Instead, we shall compare their solitary-wave solutions, which, for the MCC system, have been compared to experiments.

4.1. Solitary waves of Boussinesq MCC

To find solitary waves of the Boussinesq MCC, we first look for traveling-wave solutions by letting $h(t,x) = h(\xi)$ and $w(t,x) = w(\xi)$, where $\xi \equiv x - ct$ for a constant speed c to be determined. Then, (16) and (17) become

$$-ch_\xi + \left[(1-h^2)w\right]_\xi = 0, \tag{30}$$

$$-cw_\xi + \left[(1-w^2)h\right]_\xi = \frac{1}{24}\left(\frac{1}{1+h}\left[(1+h)^3\Gamma_2\right]_\xi - \frac{1}{1-h}\left[(1-h)^3\Gamma_1\right]_\xi\right), \tag{31}$$

where

$$\Gamma_1 \equiv c\,[(1+h)w]_{\xi\xi} + [(1+h)w]\,[(1+h)w]_{\xi\xi} - \left([(1+h)w]_{\xi}\right)^2,$$

$$\Gamma_2 \equiv -c\,[(1-h)w]_{\xi\xi} + [(1-h)w]\,[(1-h)w]_{\xi\xi} - \left([(1-h)w]_{\xi}\right)^2.$$

Integrating (30) once with respect to ξ yields

$$-ch + (1-h^2)w - C_1 = 0, \tag{32}$$

where

$$C_1 \equiv -ch_0 + (1-h_0^2)w_0$$

is obtained by assuming that

$$\lim_{\xi\to\pm\infty}(h, w) = (h_0, w_0).$$

Then, we solve (32) for w and get

$$w = \frac{C_1 + ch}{1-h^2}. \tag{33}$$

Substituting this expression in (31) yields

$$-c\left(\frac{C_1+ch}{1-h^2}\right)_{\xi} + \left(\left[1-\left(\frac{C_1+ch}{1-h^2}\right)^2\right]h\right)_{\xi}$$
$$= \frac{1}{24}\left(\frac{1}{1+h}\left[(1+h)^3\Gamma_2\right]_{\xi} - \frac{1}{1-h}\left[(1-h)^3\Gamma_1\right]_{\xi}\right), \tag{34}$$

where

$$\Gamma_1 = \frac{C_1+c}{1-h}\cdot\left(\frac{C_1+ch}{1-h}\right)_{\xi\xi} - \left[\left(\frac{C_1+ch}{1-h}\right)_{\xi}\right]^2,$$

$$\Gamma_2 = \frac{C_1-c}{1+h}\cdot\left(\frac{C_1+ch}{1+h}\right)_{\xi\xi} - \left[\left(\frac{C_1+ch}{1+h}\right)_{\xi}\right]^2.$$

This allows us to solve for h first and find w using (33) later if desired. While (34) seems complicated, it can be integrated. Integrating once

$$-c\cdot\frac{C_1+ch}{1-h^2} + \left[1-\left(\frac{C_1+ch}{1-h^2}\right)^2\right]h - C_2$$
$$= \frac{(C_1-c)^2}{48}\left[\left(\frac{h_{\xi}}{1+h}\right)^2 - \frac{2h_{\xi\xi}}{1+h}\right] - \frac{(C_1+c)^2}{48}\left[\left(\frac{h_{\xi}}{1-h}\right)^2 + \frac{2h_{\xi\xi}}{1-h}\right], \tag{35}$$

where

$$C_2 \equiv -cw_0 + (1 - w_0^2)h_0 = -c \cdot \frac{C_1 + ch_0}{1 - h_0^2} + \left[1 - \left(\frac{C_1 + ch_0}{1 - h_0^2}\right)^2\right] h_0$$

is obtained by assuming that solutions decay at infinity:

$$\lim_{\xi \to \pm\infty} h_\xi = \lim_{\xi \to \pm\infty} h_{\xi\xi} = 0.$$

Multiplying (35) by $-2h_\xi$ and integrating again, one obtains

$$\frac{(C_1 + ch)^2}{1 - h^2} - h^2 + 2C_2 h - C_3 = \frac{(C_1 - c)^2}{24} \cdot \frac{h_\xi^2}{1 + h} + \frac{(C_1 + c)^2}{24} \cdot \frac{h_\xi^2}{1 - h}, \tag{36}$$

where

$$C_3 \equiv \frac{(C_1 + ch_0)^2}{1 - h_0^2} - h_0^2 + 2C_2 h_0.$$

Equation (36) is of the form

$$h_\xi^2 + V_c = 0 \tag{37}$$

with

$$V_c(h) \equiv -\frac{12(h - h_0)^2 Q_c(h)}{\left[\left(1 - h_0^2\right) w_0 + c\,(h - h_0)\right]^2 + c^2\left(1 - h^2\right)},$$

where Q_c is a monic second-degree polynomial in h with roots

$$h^\pm \equiv -(c + h_0 w_0)w_0 \pm \sqrt{[1 - (c + h_0 w_0)^2](1 - w_0^2)}. \tag{38}$$

A solitary-wave, i.e., localized, solution of (37) corresponds to a "potential well" of V_c. We show plots of V_c for different values of c when $h_0 = 0.4$ and $w_0 = 0.1$ in Figure 3.

In the figure:

- Typical solitary waves with speeds c^+ and c^- correspond to the potential wells of the dashed curves. The widths of the wells are the amplitudes of the solitary waves. In both cases, the solitary waves are of depression type, because h_0 is on the right of the potential wells.
- Dot–dash curves represent maximum-amplitude limits of solitary waves, the so-called "table-top" solitary waves [17, 21], with speeds c_m^+ and c_m^-.
- Solid curves correspond to zero-amplitude limits of solitary waves with speeds c_0^+ and c_0^-.

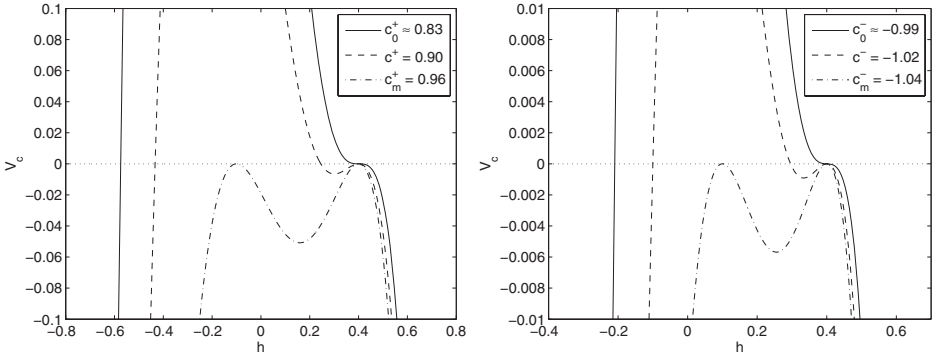

Figure 3. Plots of V_c for different values of c when $h_0 = 0.4$ and $w_0 = 0.1$.

We shall derive analytical expressions for c_m^+ and c_m^- and c_0^+ and c_0^- as functions of h_0 and w_0, thus obtaining ranges of possible solitary-wave speeds, as follows.

- c_m^+ and c_m^- are the speeds at which Q_c has a double root, i.e., $h^+ = h^-$. Consequently,

$$c_m^\pm = -h_0 w_0 \pm 1,$$

and the peaks of the table-top solitary waves are at

$$h_m^\pm \equiv -(c_m^\pm + h_0 w_0) w_0 = \mp w_0.$$

- c_0^+ and c_0^- are the speeds at which Q_c has a root at h_0, i.e., $h^+ = h_0$ or $h^- = h_0$. Consequently,

$$c_0^\pm = -2h_0 w_0 \pm \sqrt{\left(1 - h_0^2\right)\left(1 - w_0^2\right)}.$$

Below, we shall see that $c_0^\pm$ are also the linear speeds in the KdV equations associated with the stable model and Boussinesq MCC.

It is straightforward to check that $c_0^+ \le c_m^+$ and $c_m^- \le c_0^-$. Thus, possible speeds c^+ and c^- of right-going and left-going solitary waves, respectively, satisfy the inequalities

$$c_m^+ \ge c^+ \ge c_0^+ \qquad \text{and} \qquad c_m^- \le c^- \le c_0^-.$$

Figure 4 gives an interpretation of these two inequalities for $h_0 = 0.4$. Solid lines represent c_m^+ and c_m^-, while solid curves represent c_0^+ and c_0^- for as functions of w_0. The shaded regions correspond to possible solitary-wave speeds c^+ and c^-. Vertical dotted lines bound the range of w_0 for which the stable model is stable for the given h_0, i.e., $\alpha \ge 0$. We note that this range of w_0 corresponds to the conditions $c_0^+ \ge 0$ and $c_0^- \le 0$.

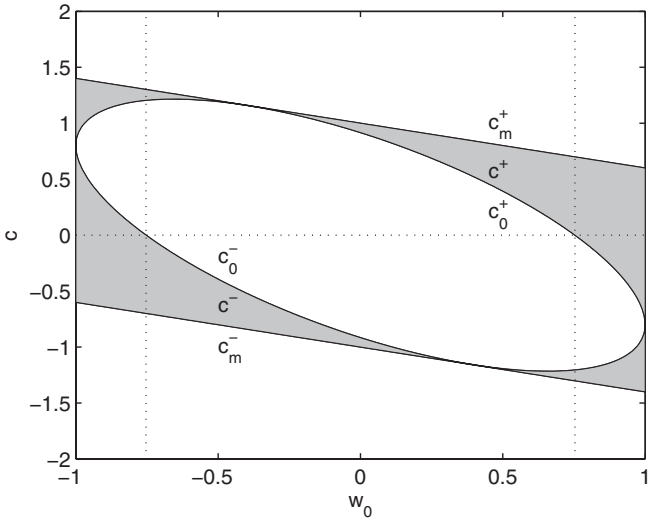

Figure 4. Possible solitary-wave speeds for $h_0 = 0.4$.

4.2. Solitary waves of the stable model

To find solitary waves of the stable model, we follow a procedure similar to that in the previous section. We first look for traveling-wave solutions by letting $h(t, x) = h(\xi)$ and $w(t, x) = w(\xi)$, where $\xi \equiv x - ct$ for a constant speed c to be determined. Then, (28) and (29) with μ^2 absorbed become

$$-ch_\xi + \left[(1-h^2)w\right]_\xi = 0, \tag{39}$$

$$-cw_\xi + \left[(1-w^2)h\right]_\xi = \frac{c}{12}\left[2h_0w_0(1-\beta)h_{\xi\xi\xi} - (1-h_0^2)(1+\beta)w_{\xi\xi\xi}\right]. \tag{40}$$

Integrating (39) and (40) once with respect to ξ yields

$$-ch + (1-h^2)w - C_1 = 0, \tag{41}$$

$$-cw + (1-w^2)h - C_2 = \frac{c}{12}\left[2h_0w_0(1-\beta)h_{\xi\xi} - (1-h_0^2)(1+\beta)w_{\xi\xi}\right]. \tag{42}$$

Then, we solve (41) for w and substitute it in (42) to obtain

$$-c\cdot\frac{C_1+ch}{1-h^2} + \left[1-\left(\frac{C_1+ch}{1-h^2}\right)^2\right]h - C_2$$

$$= \frac{c}{6}\left[2h_0w_0(1-\beta)h_{\xi\xi} - \left(1-h_0^2\right)(1+\beta)\left(\frac{C_1+ch}{1-h^2}\right)_{\xi\xi}\right], \qquad (43)$$

We cannot integrate (43) once more to perform an analysis similar to that in the previous section. However, we can understand its behavior on the (h, h_ξ) phase plane by rewriting it as a system of equations

$$h_\xi = s, \qquad (44)$$

$$s_\xi = F_c + G_c s^2, \qquad (45)$$

where

$$F_c(h) \equiv \frac{6}{c}\cdot\frac{(1-h^2)^2(h-C_2) - (C_1+ch)(c+C_1h)}{2h_0w_0(1-\beta)(1-h^2)^2 - (1-h_0^2)(1+\beta)(c+2C_1h+ch^2)},$$

$$G_c(h) \equiv \frac{1}{1-h^2}\cdot\frac{(1-h_0^2)(1+\beta)(C_1+3ch+3C_1h^2+ch^3)}{2h_0w_0(1-\beta)(1-h^2)^2 - (1-h_0^2)(1+\beta)(c+2C_1h+ch^2)}.$$

Clearly, any point of the form $(h^*, 0)$, where h^* is a root of F_c, is a fixed point of the system (44)–(45). We linearize this system around the fixed point to obtain

$$h_\xi = s, \qquad (46)$$

$$s_\xi = F_c'(h^*)(h-h^*). \qquad (47)$$

The system (46)–(47) has eigenvalues $\pm\sqrt{F_c'(h^*)}$, thus

- the fixed point $(h^*, 0)$ is a saddle when $F_c'(h^*) > 0$,
- the fixed point $(h^*, 0)$ is a center when $F_c'(h^*) < 0$.

Figures 5 and 6 show, superimposed, the phase-plane plots (in solid curves) with graphs of F_c (in dashed curves) for different values of $c > 0$ when $h_0 = 0.4$ and $w_0 = 0.1$.

- In each of Figures 5(a) and (b), a typical solitary wave corresponds to a homoclinic orbit joining the saddle $(h_0, 0)$ with itself. Another point where the orbit crosses the dotted line $h_\xi = 0$ corresponds to the peak of the solitary wave. Thus, Figure 5(a) represents a deeper solitary wave of depression type than that in Figure 5(b).
- In Figure 6(a), a table-top solitary wave corresponds to a heteroclinic cycle joining the saddle $(h_0, 0)$ with another saddle. We note that $c \approx 0.959$ is very close to $c_m^+ = 0.96$ for the Boussinesq MCC.

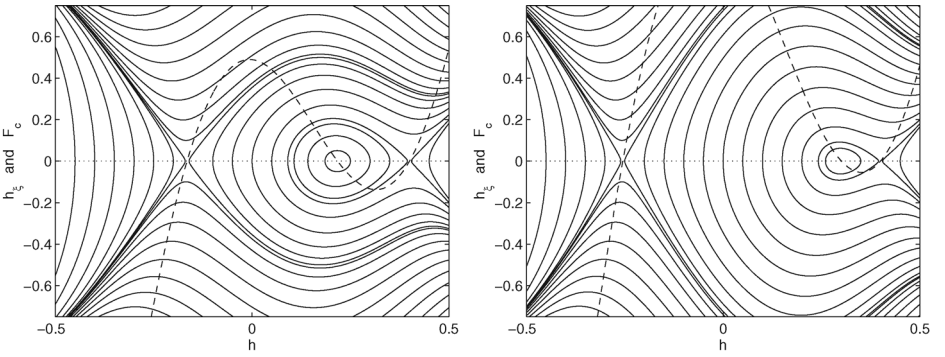

(a) $c = 0.94$ (b) $c = 0.90$

Figure 5. Phase–plane plots and graphs of F_c for $h_0 = 0.4$ and $w_0 = 0.1$.

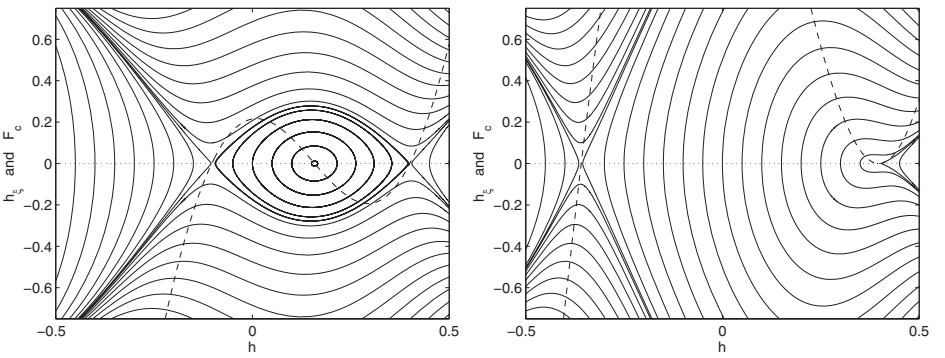

(a) $c \approx 0.959$ (b) $c \approx 0.836$

Figure 6. Phase–plane plots and graphs of F_c for $h_0 = 0.4$ and $w_0 = 0.1$.

- Figure 6(b) represents the zero-amplitude limit. Now $F_c'(h_0) = 0$, and the integral curve approaching the fixed point $(h_0, 0)$ is a cusp. We note again that $c \approx 0.836$ is very close to $c_0^+ \approx 0.83$ for the Boussinesq MCC.

4.3. Comparison of solitary waves

If (h_0, w_0, c, h) satisfies (37) or (43), then it is straightforward to check that

$$(-h_0, w_0, -c, -h), \qquad (h_0, -w_0, -c, h), \qquad (-h_0, -w_0, c, h)$$

satisfy the same equation. Thus, it suffices to compare solitary waves of the Boussinesq MCC and the stable model for nonnegative h_0 and w_0. Solitary waves in Figures (7)–(10) are computed on the spatial domain $[-100, 100)$, but only the middle fifth of this domain is shown.

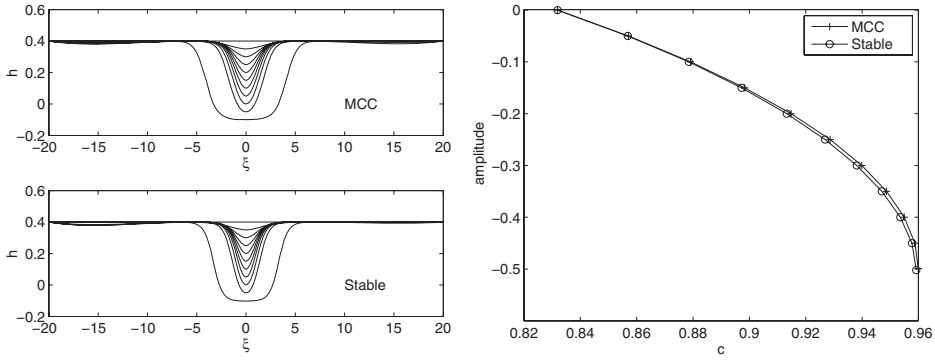

Figure 7. Right-going solitary waves of the Boussinesq MCC and the stable model when $h_0 = 0.4$ and $w_0 = 0.1$.

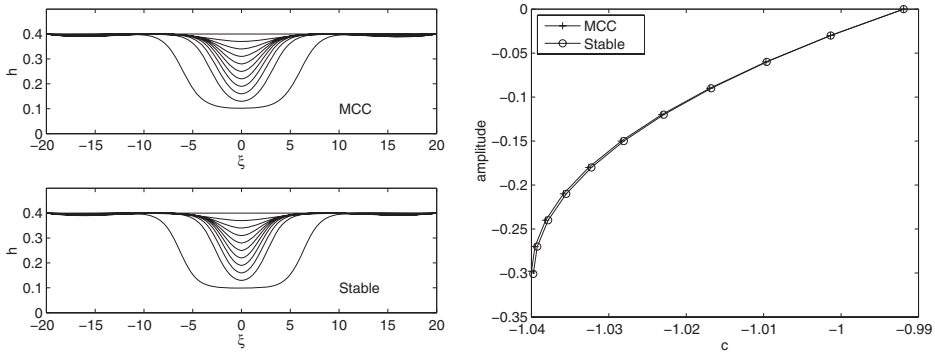

Figure 8. Left-going solitary waves of the Boussinesq MCC and the stable model when $h_0 = 0.4$ and $w_0 = 0.1$.

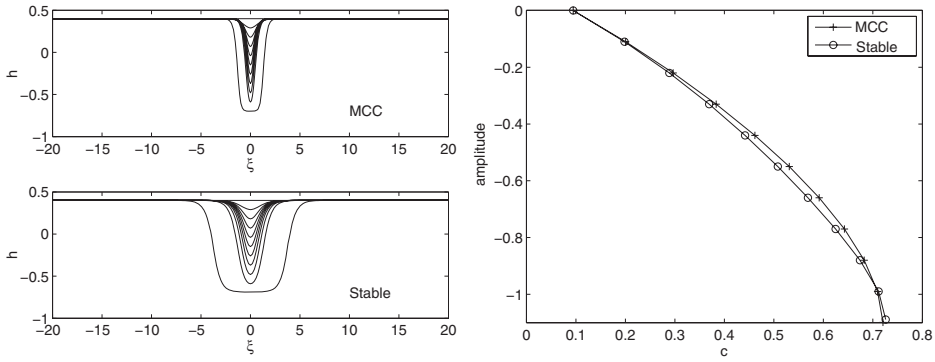

Figure 9. Right-going solitary waves of the Boussinesq MCC and the stable model when $h_0 = 0.4$ and $w_0 = 0.7$.

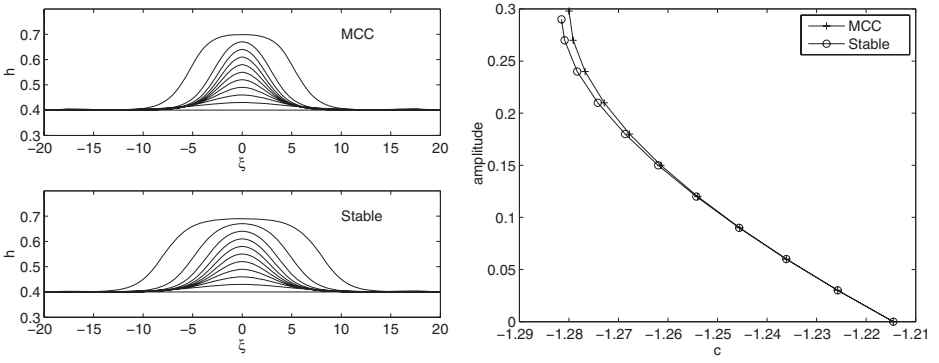

Figure 10. Left-going solitary waves of the Boussinesq MCC and the stable model when $h_0 = 0.4$ and $w_0 = 0.7$.

Figure 7 shows right-going solitary waves of the Boussinesq MCC and the stable model when $h_0 = 0.4$ and $w_0 = 0.1$. On the left, solitary waves with different amplitudes are shown, and those with maximum amplitudes are table-top solitary waves. The peaks of the table-top solitary waves are very close to $h_m^+ = -0.1$, as expected from the foregoing discussion on Boussinesq MCC solitary waves. On the right, plots of amplitudes of solitary waves versus their speeds are shown. The speeds of the table-top solitary waves are very close to $c_m^+ = 0.96$ as expected. The speeds of the zero-amplitude limits of solitary waves are not obtained from our computation, but rather the value c_0^+ for the Boussinesq MCC is used to complete the plots.

Figure 8 shows left-going solitary waves in the same setting. The peaks and the speeds of the table-top solitary waves are very close to $h_m^- = 0.1$ and $c_m^- = -1.04$, respectively, as expected. The value c_0^- for the Boussinesq MCC is used for the speeds of the zero-amplitude limits of solitary waves to complete the plots on the right.

We now compare solitary waves of the Boussinesq MCC and the stable model in the presence of strong background shear. Figure 9 shows right-going solitary waves when $h_0 = 0.4$ and $w_0 = 0.7$. While the stable model captures well the maximum amplitudes and speed–amplitude curve, we see that solitary waves of the stable model are noticeably broader than those of the Boussinesq MCC. This could be expected, because the solitary waves have large amplitudes, and the linearized dispersion of the stable model is no longer a good approximation to that of the Boussinesq MCC.

Figure 10 shows left-going solitary waves in the same setting. These solitary waves are different from those that we have seen thus far, because they are of elevation type. When $h_0 > 0$, i.e., when the lower fluid layer is thicker than the upper fluid layer, solitary waves of depression type are more common. However, when background shear is sufficiently strong, left-going solitary

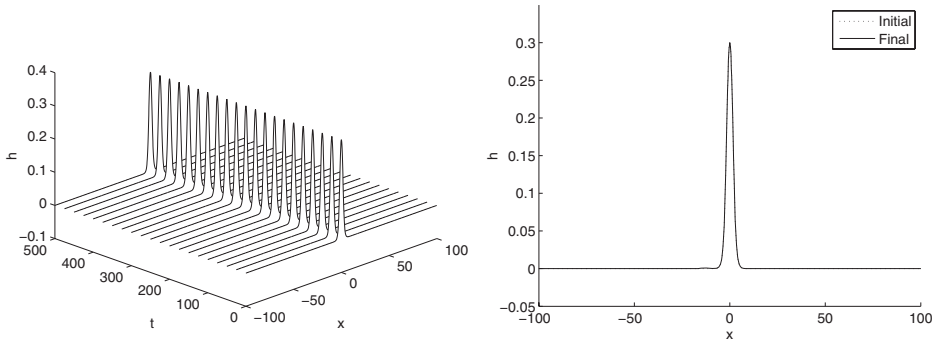

Figure 11. A solitary wave of the stable model when $h_0 = 0$ and $w_0 = -0.4$ is used as initial data for the stable model (28)–(29). Final time: $t = 500$.

waves will be of elevation type. Since $h_m^- = w_0$ for the Boussinesq MCC, this phenomenon takes place when $w_0 > h_0$.

In conclusion, the stable model captures the essential features of solitary waves extremely well. Given its simplicity for the sample time-dependent computations shown below, we believe that it is an appropriate model for long interfacial waves.

4.4. Time-dependent solutions

In this section, we compute time-dependent solutions to the stable model (28)–(29). Solutions are computed with a pseudospectral scheme and fourth-order Runge–Kutta integration in time. In Figure 11, a solitary wave of the stable model when $h_0 = 0$ and $w_0 = -0.4$ with amplitude 0.3 and speed $c \approx 0.995$ is used as initial data. On the left, solutions at different points in time are shown in the frame of reference moving with the speed c. On the right, the initial data and the solution at final time $t = 500$ are compared. As expected, the solitary wave of the stable model maintains its shape and speed, and the initial data and the solution at the final time coincide without any sign of instability (as would be evident in an MCC computation without filtering). Periodic boundary conditions are assumed on the spatial domain $[-200, 200)$, but only the middle half of this domain is shown.

In Figure 12, a solitary wave of the Boussinesq MCC when $h_0 = 0$ and $w_0 = -0.4$ with amplitude 0.3 and speed $c \approx 0.994$ is used as initial data for the stable model (28)–(29). On the left, solutions at different points in time are shown in the frame of reference moving with the speed c. Since the initial data is *not* a solitary wave of the stable model (but is close to one), there is energy radiation in the direction opposite its motion. This radiation stops after a finite time, and the solution now consists of a solitary wave of the stable model followed by a receding train of small oscillations. On the right, the initial data

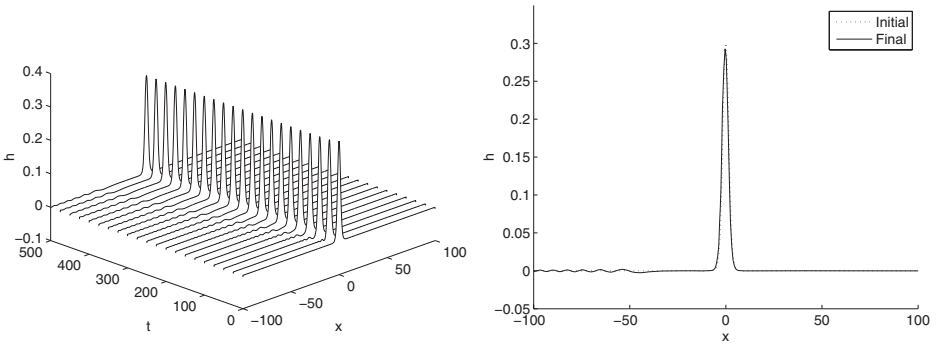

Figure 12. A solitary wave of the Boussinesq MCC when $h_0 = 0$ and $w_0 = -0.4$ is used as initial data for the stable model (28)–(29). Final time: $t = 500$.

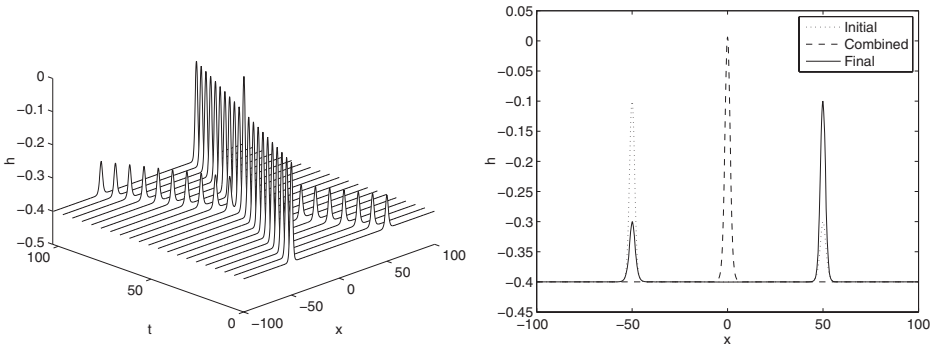

Figure 13. A head-on collision of solitary waves of the stable model when $h_0 = -0.4$ and $w_0 = 0$. Final time: $t \approx 102$.

and the solution at final time $t = 500$ are compared. We note slight losses in amplitude and speed of the new solitary wave compared to the initial data. Again, only the middle half of the spatial domain $[-200, 200)$ is shown.

An important property of solitary waves is that, except for possible phase shifts, they change very little after emerging from collisions with other solitary waves. Figure 13 shows a head-on collision of solitary waves of the stable model when $h_0 = -0.4$ and $w_0 = 0$. The larger solitary wave has amplitude 0.3 and speed $c \approx 0.994$, while the smaller solitary wave has amplitude 0.1 and speed $c \approx -0.954$. On the left, solutions at different points in time are shown in the frame of reference moving with the average speed. On the right, we compare the initial data, the solution when the solitary waves combine at $t \approx 51$, and the solution at final time $t \approx 102$, which is approximately twice the initial separation between the solitary waves divided by the average speed. Very little change in the shapes of both solitary waves is seen after the collision. The fact that the peak of the larger solitary wave at the final time aligns with

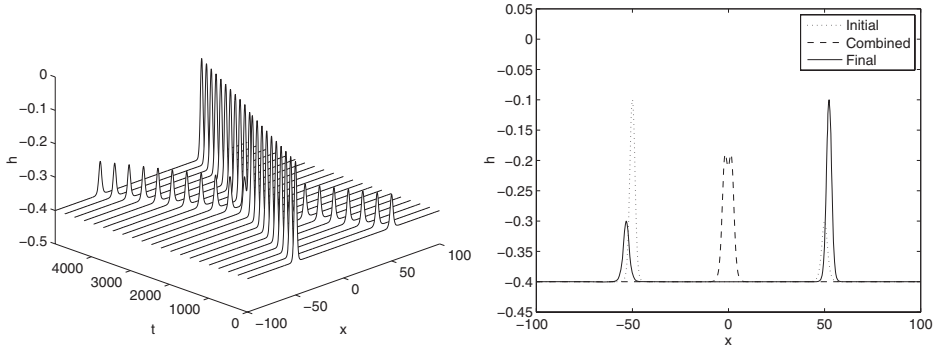

Figure 14. An overtaking collision of solitary waves of the stable model when $h_0 = -0.4$ and $w_0 = 0$. Final time: $t \approx 4926$.

the peak of the smaller solitary wave at the initial time (and vice versa) means that there is very little phase shift, as expected, during the collision.

Figure 14 shows an overtaking collision of solitary waves of the stable model when $h_0 = -0.4$ and $w_0 = 0$. The larger solitary wave has amplitude 0.3 and speed $c \approx 0.994$, while the smaller solitary wave has amplitude 0.1 and speed $c \approx 0.954$. On the left, solutions at different points in time are shown in the frame of reference moving with the average speed. On the right, we compare the initial data, the solution when the solitary waves combine at $t \approx 2395$, and the solution at final time $t \approx 4926$, which is approximately twice the initial separation between the solitary waves divided by the average speed. We see very little change in the shapes of both solitary waves after the collision. However, the fact that the peaks of the solitary waves do not align means that there are, as expected, significant phase shifts during the collision. Also, note that the profile of the combined solitary waves is different during head-on and the overtaking collisions.

5. The KdV equation

Unidirectional small and moderate amplitude internal waves are often modeled by the KdV and modified KdV (mKdV) equations [22]. Here, a KdV equation associated with the stable model (28)–(29) can be derived by keeping only linear and quadratic terms in the hyperbolic part of the equation and seeking waves traveling in one direction only. We assume that these nonlinear quadratic terms are of the same order as existing linear dispersive terms. This yields

$$\tilde{h}_t - 2h_0 w_0 \tilde{h}_x + (1 - h_0^2)\tilde{w}_x = 2\mu^2 \left[h_0 (\tilde{h}\tilde{w})_x + w_0 \tilde{h}\tilde{h}_x \right], \tag{48}$$

$$\tilde{w}_t + (1 - w_0^2)\tilde{h}_x - 2h_0 w_0 \tilde{w}_x = 2\mu^2 \left[w_0(\tilde{h}\tilde{w})_x + h_0 \tilde{w}\tilde{w}_x \right]$$
$$-\frac{\mu^2}{12}\left[2h_0 w_0 \tilde{h}_{xxt} - (1 - h_0^2)\tilde{w}_{xxt} + (1 - h_0^2) w_0^2 \tilde{h}_{xxx} \right], \qquad (49)$$

where

$$\tilde{h} \equiv \frac{h - h_0}{\mu^2} \qquad \text{and} \qquad \tilde{w} \equiv \frac{w - w_0}{\mu^2}.$$

The $O(1)$ terms in (48) and (49) can be decoupled into a right-going part R and a left-going part L defined by

$$R \equiv \frac{\tilde{h}}{\sqrt{1 - h_0^2}} + \frac{\tilde{w}}{\sqrt{1 - w_0^2}} \qquad \text{and} \qquad L \equiv \frac{\tilde{h}}{\sqrt{1 - h_0^2}} - \frac{\tilde{w}}{\sqrt{1 - w_0^2}}.$$

Combining Equations (48) and (49), and defining $a \equiv \sqrt{1 - h_0^2}$ and $b \equiv \sqrt{1 - w_0^2}$, one obtains equations for R and L, respectively,

$$R_t + c_0^+ R_x = \frac{\mu^2}{4}\left[(a w_0 + b h_0)(3R^2 - L^2)_x + 2(a w_0 - b h_0)(RL)_x \right]$$
$$+\frac{\mu^2}{24}\frac{a}{b}\left[c_0^+ R_{xxt} + c_0^- L_{xxt} - a^2 w_0^2 (R_{xxx} + L_{xxx}) \right], \qquad (50)$$

$$L_t + c_0^- L_x = \frac{\mu^2}{4}\left[(a w_0 - b h_0)(3L^2 - R^2)_x + 2(a w_0 + b h_0)(RL)_x \right]$$
$$-\frac{\mu^2}{24}\frac{a}{b}\left[c_0^+ R_{xxt} + c_0^- L_{xxt} - a^2 w_0^2 (R_{xxx} + L_{xxx}) \right]. \qquad (51)$$

A unidirectional equation consistent with the order of the approximation can be obtained by choosing, say, $R = O(1)$, $L = O(\mu^2)$, resulting in

$$R_t + c_0^+ R_x = \frac{\mu^2}{4}(a w_0 + b h_0)(3R^2)_x + \frac{\mu^2}{24}\frac{a}{b}\left[c_0^+ R_{xxt} - a^2 w_0^2 R_{xxx} \right], \qquad (52)$$

together with an inhomogeneous equation for μ^2 corrections arising from L. To transform (52) into a standard KdV equation, define $\tilde{R}(\tilde{t}, \tilde{x}) \equiv R(t, x)$, where

$$\tilde{x} \equiv x - c_0^+ t \qquad \text{and} \qquad \tilde{t} \equiv \mu^2 t.$$

In terms of the new variables, one obtains the right-going KdV equation associated with the Boussinesq MCC

$$\tilde{R}_{\tilde{t}} - \frac{3}{2}\left(h_0\sqrt{1 - w_0^2} + w_0\sqrt{1 - h_0^2} \right)\tilde{R}\tilde{R}_{\tilde{x}}$$

$$+\frac{1}{24}\sqrt{\frac{1-h_0^2}{1-w_0^2}}\left[(c_0^+)^2+(1-h_0^2)w_0^2\right]\tilde{R}_{\tilde{x}\tilde{x}\tilde{x}}=0. \tag{53}$$

Similarly, assuming small right-going waves, the left-going KdV equation associated with the Boussinesq MCC can be obtained, yielding

$$\tilde{L}_{\tilde{t}}-\frac{3}{2}\left(h_0\sqrt{1-w_0^2}-w_0\sqrt{1-h_0^2}\right)\tilde{L}\tilde{L}_{\tilde{x}}$$
$$-\frac{1}{24}\sqrt{\frac{1-h_0^2}{1-w_0^2}}\left[(c_0^-)^2+(1-h_0^2)w_0^2\right]\tilde{L}_{\tilde{x}\tilde{x}\tilde{x}}=0, \tag{54}$$

where the linear speed in the definition of $\tilde{x}$ must be changed to c_0^-. Note that due to shear, the left–right symmetry of the KdV equations is broken. It is simple to show that the KdV equations associated with the Boussinesq MCC (16)–(17) are identical to these.

5.1. Modified KdV equation

If $h_0\approx -w_0$, then the coefficient of the quadratic term in the right-going KdV equation (53) is small. Thus, the dominant balance in the KdV equation should include cubic terms from the hyperbolic part of the stable model (or Boussinesq MCC). Thus, we proceed keeping the full cubic nonlinearity of the hyperbolic part (but expanding it about a given state) and assuming that the cubic corrections are of the same order as existing linear dispersive terms. This results in

$$\tilde{h}_t-2h_0w_0\tilde{h}_x+(1-h_0^2)\tilde{w}_x=2\mu\left[h_0(\tilde{h}\tilde{w})_x+w_0\tilde{h}\tilde{h}_x\right]+\mu^2(\tilde{h}^2\tilde{w})_x$$
$$\tilde{w}_t+(1-w_0^2)\tilde{h}_x-2h_0w_0\tilde{w}_x=2\mu\left[w_0(\tilde{h}\tilde{w})_x+h_0\tilde{w}\tilde{w}_x\right]+\mu^2(\tilde{h}\tilde{w}^2)_x$$
$$-\frac{\mu^2}{12}\left[2h_0w_0\tilde{h}_{xxt}-(1-h_0^2)\tilde{w}_{xxt}\right.$$
$$\left.+(1-h_0^2)w_0^2\tilde{h}_{xxx}\right],$$

where

$$\tilde{h}\equiv\frac{h-h_0}{\mu}\qquad\text{and}\qquad\tilde{w}\equiv\frac{w-w_0}{\mu}.$$

Consequently,

$$R_t+c_0^+R_x=\frac{\mu}{4}\left[(aw_0+bh_0)(3R^2-L^2)_x+2(aw_0-bh_0)(RL)_x\right]$$
$$+\frac{\mu^2}{4}ab(R^3-L^2R)_x$$

$$+\frac{\mu^2}{24}\frac{a}{b}\left[c_0^+ R_{xxt} + c_0^- L_{xxt} - a^2 w_0^2 (R_{xxx} + L_{xxx})\right],$$

$$L_t + c_0^- L_x = \frac{\mu}{4}\left[(aw_0 - bh_0)(3L^2 - R^2)_x + 2(aw_0 + bh_0)(RL)_x\right]$$

$$+\frac{\mu^2}{4} ab(LR^2 - L^3)_x$$

$$-\frac{\mu^2}{24}\frac{a}{b}\left[c_0^+ R_{xxt} + c_0^- L_{xxt} - a^2 w_0^2 (R_{xxx} + L_{xxx})\right].$$

Assuming that the coefficient of the quadratic advective nonlinearity is small, consider $aw_0 + bh_0 = \mu q$ with q order 1. Then,

$$R_t + c_0^+ R_x = \frac{\mu}{2}(aw_0 - bh_0)(RL)_x$$

$$+\frac{\mu^2}{4}\left[q(3R^2 - L^2)_x + ab(R^3 - L^2 R)_x\right]$$

$$+\frac{\mu^2}{24}\frac{a}{b}\left[c_0^+ R_{xxt} + c_0^- L_{xxt} - a^2 w_0^2 (R_{xxx} + L_{xxx})\right],$$

$$L_t + c_0^- L_x = \frac{\mu}{4}(aw_0 - bh_0)(3L^2 - R^2)_x$$

$$+\frac{\mu^2}{4}\left[2q(RL)_x + ab(LR^2 - L^3)_x\right]$$

$$-\frac{\mu^2}{24}\frac{a}{b}\left[c_0^+ R_{xxt} + c_0^- L_{xxt} - a^2 w_0^2 (R_{xxx} + L_{xxx})\right].$$

Making the assumption of principally unidirectional propagation with $R = O(1)$ and $L \to \mu L$, then

$$R_t + c_0^+ R_x = \frac{\mu^2}{4}\left[2(aw_0 - bh_0)(RL)_x + q(3R^2)_x + ab(R^3)_x\right]$$

$$+\frac{\mu^2}{24}\frac{a}{b}\left[c_0^+ R_{xxt} - a^2 w_0^2 R_{xxx}\right],$$

$$L_t + c_0^- L_x = -\frac{1}{4}(aw_0 - bh_0)(R^2)_x.$$

To leading order, $R(x - c_0^+ t)$ and the second equation can be solved, with

$$L = \frac{1}{4(c_0^+ - c_0^-)}(aw_0 - bh_0)(R^2).$$

Substituting this into the first equation yields

$$R_t + c_0^+ R_x = \frac{\mu^2}{4}\left[q(3R^2)_x + (ab - w_0 h_0)(R^3)_x\right]$$

$$+\frac{\mu^2}{24}\frac{a}{b}\left[c_0^+ R_{xxt} - a^2 w_0^2 R_{xxx}\right].$$

Finally, rewriting the equation in the moving frame for $\tilde{R}(\tilde{t}, \tilde{x}) \equiv R(t, x)$, where

$$\tilde{x} \equiv x - c_0^+ t \qquad \text{and} \qquad \tilde{t} \equiv \mu^2 t,$$

one obtains the right-going modified KdV equation associated with the stable model:

$$\tilde{R}_{\tilde{t}} - \frac{3}{2} q \tilde{R} \tilde{R}_{\tilde{x}} - \frac{3}{4} \tilde{R}^2 \tilde{R}_{\tilde{x}} + \frac{1}{24}(1 + 3h_0^2)\tilde{R}_{\tilde{x}\tilde{x}\tilde{x}} = 0.$$

When $q = 0$, this equation is of the defocusing form, a case in which there are no solitary-wave solutions. This is expected, since the condition $q = 0$ implies that $c_m^+ = c_0^+$, and there should be no right-going solitary wave. A similar derivation can be carried out for left-going modes. Of course, the modified KdV equation associated with the stable model or the Boussinesq MCC is identical.

6. Conclusion

The system of equations describing fully nonlinear long internal waves obtained under the Boussinesq approximation is mathematically ill-posed despite the fact that physically stable internal waves have been observed. To remedy this problem, we have performed an exchange of spatial and temporal derivatives in a dispersive term to obtain a stable and computationally inexpensive model that is equal to the Boussinesq MCC in its hyperbolic part and asymptotically equivalent to the linearized Boussinesq MCC in the dispersive part. To see how closely our stable model approximates the Boussinesq MCC, we have studied and compared their solitary waves and found that they show good agreement in speed–amplitude relations and in all but one profile width with large background shear. Previous works have studied solitary waves of the MCC without background shear and found that the solitary waves cannot cross the midlevel and that only solitary waves of depression type are possible when the lower fluid layer is thicker than the upper fluid layer. Including a stable background shear, we found that both of these facts are false. The level which solitary waves cannot cross depends on both their direction of wave motion and the strength of the shear, and solitary waves of elevation are also possible when the lower fluid layer is thicker than the upper fluid layer. We have also obtained classical and modified KdV equations associated with the stable model.

A natural extension of this work is to study a similar regularization of a MCC model without the Boussinesq approximation. While this would allow for better comparisons with experiments, most geophysical flows are well described by the Boussinesq approximation.

Acknowledgments

The work of A. Boonkasame and P. A. Milewski was partially supported by the Division of Mathematical Sciences of the National Science Foundation, under Grant Number DMS-0908077. P. A. Milewski also thanks the generous support from a Royal Society Wolfson award.

Appendix

We recall that the system (16)–(17) is mathematically ill-posed, because the term h_{xxx} in the linearization of (17) has a destabilizing effect. Since this term originates from the terms $[(1+h)w]_{xx}$ in G_1 and $[(1-h)w]_{xx}$ in G_2, we shall replace them with stabilizing terms as follows. For convenience, let

$$v_1 \equiv (1+h)w \qquad \text{and} \qquad v_2 \equiv (1-h)w.$$

Our goal is to exchange $v_{1,x}$ and $v_{2,x}$ with h_t and w_t. To this end, we seek a 2×2 matrix $C(h,w)$ such that

$$v_x = Cu_t, \tag{A.1}$$

where $u \equiv [\,h\,,\,w\,]^\top$ and $v \equiv [\,v_1\,,\,v_2\,]^\top$. Using the chain rule, we can rewrite (A.1) as

$$Ju_x = Cu_t, \tag{A.2}$$

where J is the Jacobian of v with respect to u. On the other hand, if we ignore the right-hand side of (17), then we can rewrite this equation and (16) with an $O(\mu^2)$ error as

$$u_t + Bu_x = 0, \tag{A.3}$$

where

$$B(u) \equiv \begin{bmatrix} -2hw & 1-h^2 \\ 1-w^2 & -2hw \end{bmatrix}.$$

Next, we eliminate u_t from (A.2) and (A.3) and obtain

$$(J+CB)u_x = 0,$$

for all u_x, which implies that $J+CB=0$. The points (h,w) at which B is nonsingular satisfy the inequality $\alpha(h,w)\neq 0$, where α is defined in Section 3 At these points, $C=-JB^{-1}$, and from (A.1), we have

$$v_x = \frac{1}{\alpha}\begin{bmatrix} -2hw^2-(1+h)(1-w^2) & -(1-h^2)w-2(1+h)hw \\ 2hw^2-(1-h)(1-w^2) & (1-h^2)w-2(1-h)hw \end{bmatrix} u_t.$$

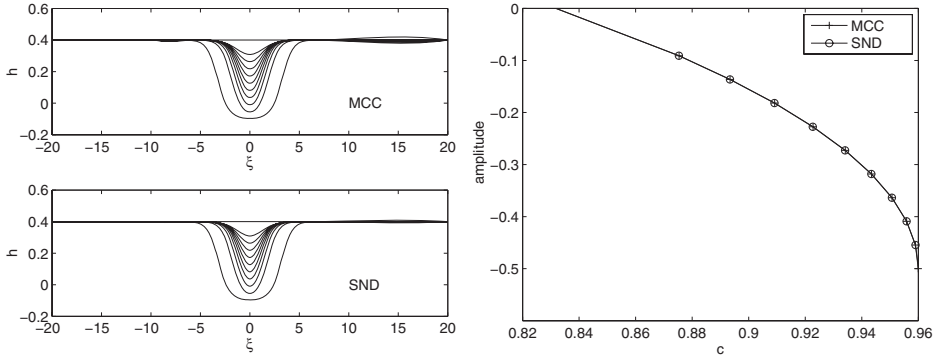

Figure 15. Right-going solitary waves of the Boussinesq MCC and the stable model with nonlinear dispersion when $h_0 = 0.4$ and $w_0 = 0.1$.

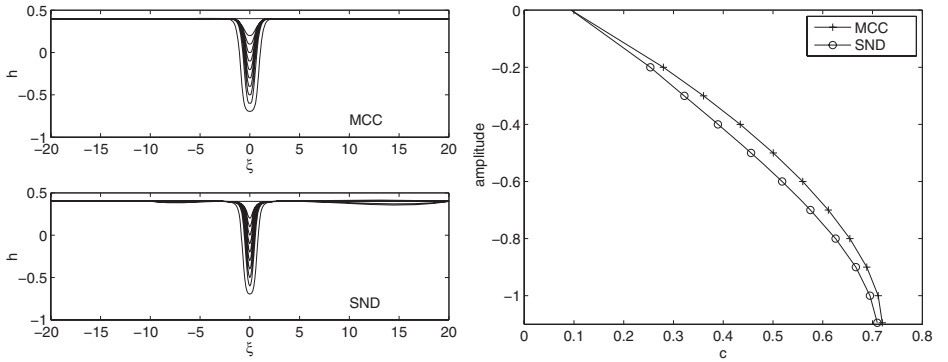

Figure 16. Right-going solitary waves of the Boussinesq MCC and the stable model with nonlinear dispersion when $h_0 = 0.4$ and $w_0 = 0.7$.

Then, we replace the terms $[(1+h)w]_{xx}$ in G_1 by $(v_{1,x})_x$ and $[(1-h)w]_{xx}$ in G_2 by $(v_{2,x})_x$ and rewrite (17) with an $O(\mu^4)$ error. Now the linearization of the modified (17) is exactly the same as (27), and we have stabilized the nonhydrostatic Boussinesq system while retaining nonlinearity in its dispersive terms. Despite its stability, evolving this system numerically is more complicated than the stable model, and we shall not pursue it. Instead, we compute solitary waves for this stable system with nonlinear dispersion (SND) and compare them to those obtained from the Boussinesq MCC in two previously computed cases.

In Figure 15, we repeat the case of Figure 7. Here, while stable system with linear dispersion was already accurate, the SND system gives a slightly improved approximation to the Boussinesq MCC.

Figure 16 shows that in the presence of strong shear, the SND system yields solitary waves that are similar in shape to those from the Boussinesq MCC, while solitary waves of the stable system with linear dispersion are much broader as shown in Figure 9.

Despite these improvements, it is not clear whether, for time-dependent solutions, the added complications of evolving the full nonlinear system are warranted.

References

1. D. R. Christie, The morning glory of the Gulf of Carpentaria, *Aust. Meteorol. Mag.* 41: 21–60 (1992).
2. R. B. Perry and G. R. Schimke, Large amplitude internal waves observed off the north-west coast of Sumatra, *J. Geophys. Res.* 70: 2319–2324 (1965).
3. D. J. Benney, Long nonlinear waves in fluid flows, *J. Math. Phys.* 45: 52–63 (1966).
4. R. Long, Long waves in a two-fluid system, *J. Meteorol.* 13: 70–74 (1956).
5. L. V. Ovsyannikov, Two-layer shallow-water model, *J. Appl. Mech. Tech. Phys.* 20: 127–135 (1979).
6. R. Liska, L. Margolin, and B. Wendroff, Nonhydrostatic two-layer models of incompressible flow, *Comp. Math. Appl.* 29: 25–37 (1995).
7. W. Choi and R. Camassa, Fully nonlinear internal waves in a two-fluid system, *J. Fluid Mech.* 396: 1–36 (1999).
8. M. Funakoshi and M. Oikawa, Long internal waves of large amplitude in a two-layer fluid, *J. Phys. Soc. Jpn.* 55: 128–144 (1986).
9. M. Miyata, An internal solitary wave of large amplitude., *La Mer.* 23: 43–48 (1985).
10. H. Michallet and E. Barthélemy, Experimental study of interfacial solitary waves, *J. Fluid Mech.* 366: 159–177 (1998).
11. T. P. Stanton and L. Ostrovsky, Observations of highly nonlinear internal solitons over the continental shelf, *Geophys. Res. Lett.* 25: 2695–2698 (1998).
12. R. Camassa, W. Choi, H. Michallet, P.-O. Rusås, and J. K. Sveen, On the realm of validity of strongly nonlinear asymptotic approximations for internal waves, *J. Fluid Mech.* 549: 1–23 (2006).
13. T.-C. Jo and W. Choi, Dynamics of strongly nonlinear internal solitary waves in shallow water, *Stud. Appl. Math.* 109: 205–227 (2002).
14. J. Grue, A. Jensen, P.-O. Rusas, and J. K. Sveen, Properties of large-amplitude internal waves, *J. Fluid Mech.* 380: 257–278 (1999).
15. A. Boonkasame and P. A. Milewski, The stability of large-amplitude shallow interfacial non-Boussinesq flows, *Stud. Appl. Math.* 128: 40–58 (2011).
16. J. L. Bona, M. Chen, and J.-C. Saut, Boussinesq equations and other systems for small amplitude long waves in nonlinear dispersive media. I: derivation and linear theory, *J. Nonlinear Sci.* 12: 283–318 (2002).
17. H. Y. Nguyen and F. Dias, A Boussinesq system for two-way propagation of interfacial waves, *Physical D* 237: 2365–2389 (2008).
18. R. Camassa, P.-O. Rusås, A. Saxena, and R. Tiron, Fully nonlinear periodic internal waves in a two-fluid system of finite depth, *J. Fluid Mech.* 652: 259–298 (2010).
19. W. Choi, R. Barros, and T.-C. Jo, A regularized model for strongly nonlinear internal solitary waves, *J. Fluid Mech.* 629: 73–85 (2009).

20. L. Chumakova, F. E. Menzaque, P. A. Milewski, R. R. Rosales, E. G. Tabak, and C. V. Turner, Stability properties and nonlinear mappings of two and three-layer stratified flows, *Stud. Appl. Math.* 122: 123–137 (2009).
21. F. Dias and J.-M. Vanden-Broeck, On internal fronts, *J. Fluid Mech.* 479: 145–154 (2003).
22. R. Grimshaw, E. Pelinovsky, and T. Talipova, The modified Korteweg-de Vries equation in the theory of large-amplitude internal waves, *Nonlinear Proc. Geophys.* 4: 237–250 (1997).

University of Wisconsin-Madison
University of Bath